Hurrah for Hussar! Comparisons of stacked data

J. Helen Isaac and Gary F. Margrave

ABSTRACT

We processed, stacked and post-stack migrated twelve data sets having combinations of four sources and three receivers. The same basic processing was applied to all data and we analysed data with and without filters. The dominant frequency of the unfiltered stacks is around 10 Hz with a steep drop off to 30-40 Hz, after which the spectra are flatter. The dynamite data show the greatest variation in power over the signal band and the least power at high frequencies.

Filtering the data to retain only frequencies of 1-10 Hz show the low-end spectra of data recorded by the 10 Hz and 4.5 Hz geophones to be similar for each corresponding source, while the Vectorseis spectra are different. In every case there is an increase in power from 1 Hz towards 10 Hz, except for the Vectorseis dynamite data. This increase is steep up to 4 Hz and fairly linear from 4 Hz to 10 Hz for the 10 Hz and 4.5 Hz geophones. The spectra are much flatter for the Vectorseis data and the Vectorseis dynamite data is different from all the others, having a peak at 6 Hz.

Phase-coherence plots show a dominant signal band that extends from about 10 Hz to 40 Hz for all sources and receivers, and up to near 60 Hz for the dynamite data. At low frequencies there is strong phase coherence down to at least 7.5 Hz and possibly to 5 Hz. On the radial filtered data there is phase coherence to 10 Hz and weak indications of coherence to 8 Hz. This removal of coherence between frequencies of 5 Hz and 8 Hz compared to the unfiltered data is attributed to the low frequency attenuation effects of the radial filter. Thus our conventional processing to remove undesired surface noise has adversely affected the phase-coherence analysis. The dynamite has more phase coherence at the high end than any of the vibroseis.

DATA ACQUISITION

The data presented in this paper were acquired at the experimental low-frequency seismic shoot at Hussar, Alberta in September, 2011. The line is 4.5 km long and runs NE-SW (Figure 1). Five sources were used (Table 1).

Table 1. Sources.

INOVA 364 vibroseis	custom low-dwell sweep 1 to 100 Hz	20 m intervals
INOVA 364 vibroseis	regular linear sweep from 1 to 100 Hz	20 m intervals
Eagle Failing vibroseis	custom low-dwell sweep 1 to 100 Hz	20 m intervals
Dynamite	2 kg at 15 m depth	20 m intervals
UofC Minivibe	regular linear sweep	20 m intervals

The first four sources produced shots at approximately 270 source locations but the UofC minivibe produced only 104 sources. The data from the minivibe is not presented in this paper. Each of these sources was recorded by five receiver lines, although only three of these extended along the entire 4.5 km (Table 2).

FIG. 1. Layout of the Hussar survey and geophysicists enjoying the view from the hill.

The Vectorseis data were recorded by GeoKinetics while the UofC recorded the other data. In this paper we present data recorded by the first three recording systems, which covered the entire line. Detailed information about the acquisition can be found in Margrave et al (this volume).

Table 2. Receivers.

448 ARAM SM7 10 Hz 3C geophones	10 m intervals
224 Sunfull 1C 4.5 Hz geophones	20 m intervals
448 Vectorseis 3C accelerometers	10 m intervals
15 Nanometrics 3C accelerometers	200 m intervals
48 ION-Sensor high-sensitivity 1C geophones	20 m intervals
27 GeoKinetics experimental geophones	

DATA COMPARISONS

We discuss stacked data from the four sources recorded by the first three receiver types in Table 2. All the data were processed with the same basic processes. The accelerometer data were integrated to become velocity data. Separate refraction statics solutions were calculated for the dynamite and vibroseis data. Each line had residual statics calculated independently to enhance the final reflections. Stacking velocities were picked for each line using the picks for one line as a template and were found to be extremely consistent between the data sets. Initially we processed the data conventionally, and included radial filtering (Henley, 1999) to attenuate high-amplitude low-frequency source-generated noise and Gabor deconvolution (Margrave and Lamoureux, 2002; Margrave et al., 2003). This filtering was later found to affect the frequency content so the stacked sections used in the following analysis have no filtering applied.

The unfiltered stacked data and their spectra from the four sources recorded by each receiver are shown in the following figures: SM7 geophones (Figure 2), the 4.5 Hz geophones (Figure 3) and the Vectorseis accelerometers (Figure 4). Each figure shows data from (a) the 364 low-dwell sweep, (b) the 364 linear sweep, (c) the Failing low-dwell sweep and (d) dynamite. All the sections show reflections in the first 2 s but the dynamite data recorded by geophones also exhibit slightly dipping reflections near 7 s and below. Noise below 9.5 s has been removed from the Vectorseis dynamite data.

In every case, the dominant frequency is around 10 Hz and there is a steep drop off to 30 Hz on the vibroseis and to 60 Hz on the dynamite data. The spectra for the INOVA 364 low dwell and linear sweeps have similar shapes and only slight differences in power, which is to be expected, as both sweeps have a flat Fourier spectrum from 1 to 100 Hz. Their spectra also show a low at 60-70 Hz and an increase towards 100 Hz. The

Failing vibroseis data show a steep drop to 40 Hz and then a gentle decline to 100 Hz. The dynamite data show the greatest dynamic range and the lowest power at high frequencies.

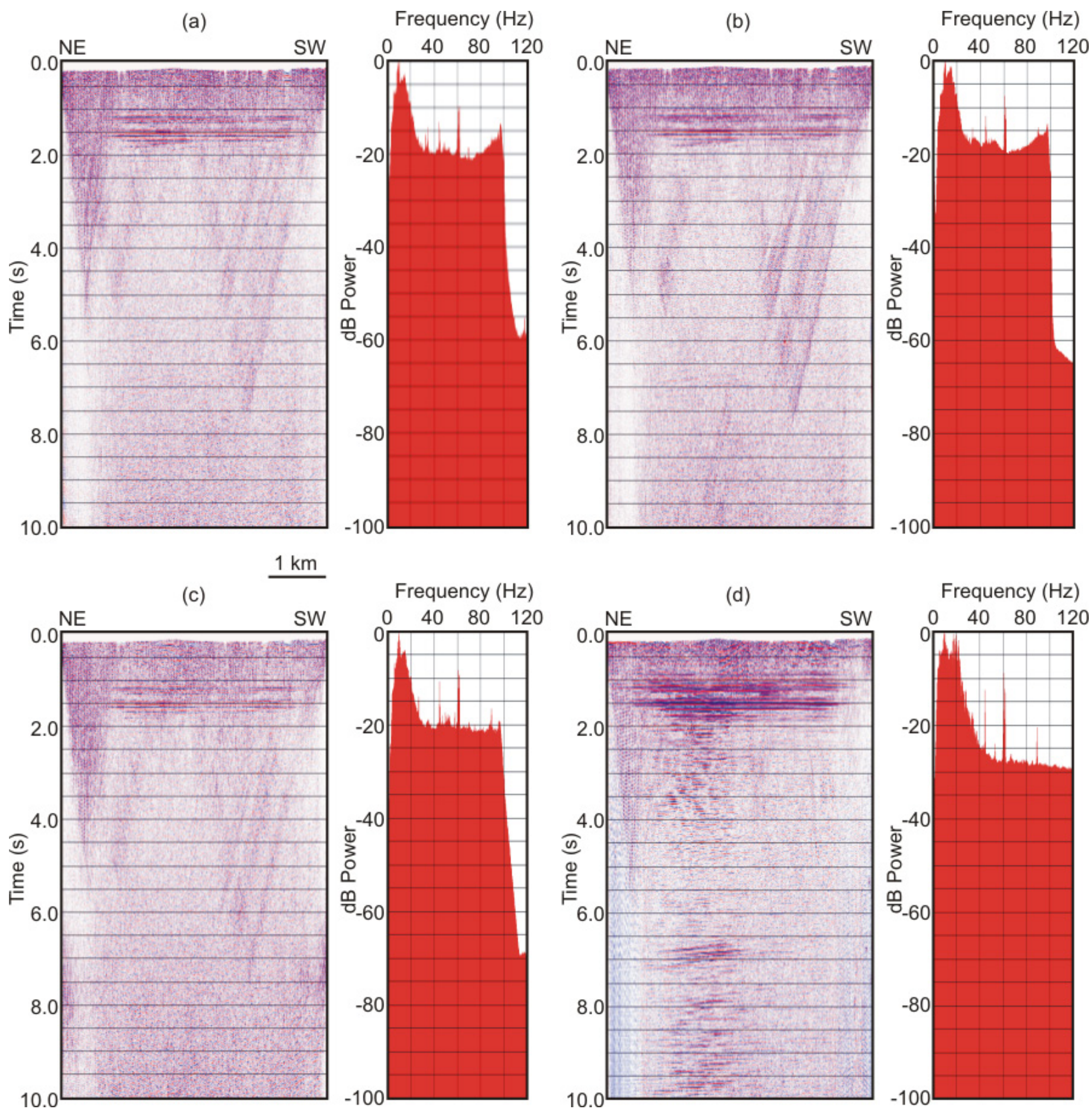

FIG. 2. Data recorded by the SM7 10 Hz geophones from (a) 364 low-dwell sweep, (b) 364 linear sweep, (c) Failing low-dwell sweep and (d) dynamite sources.

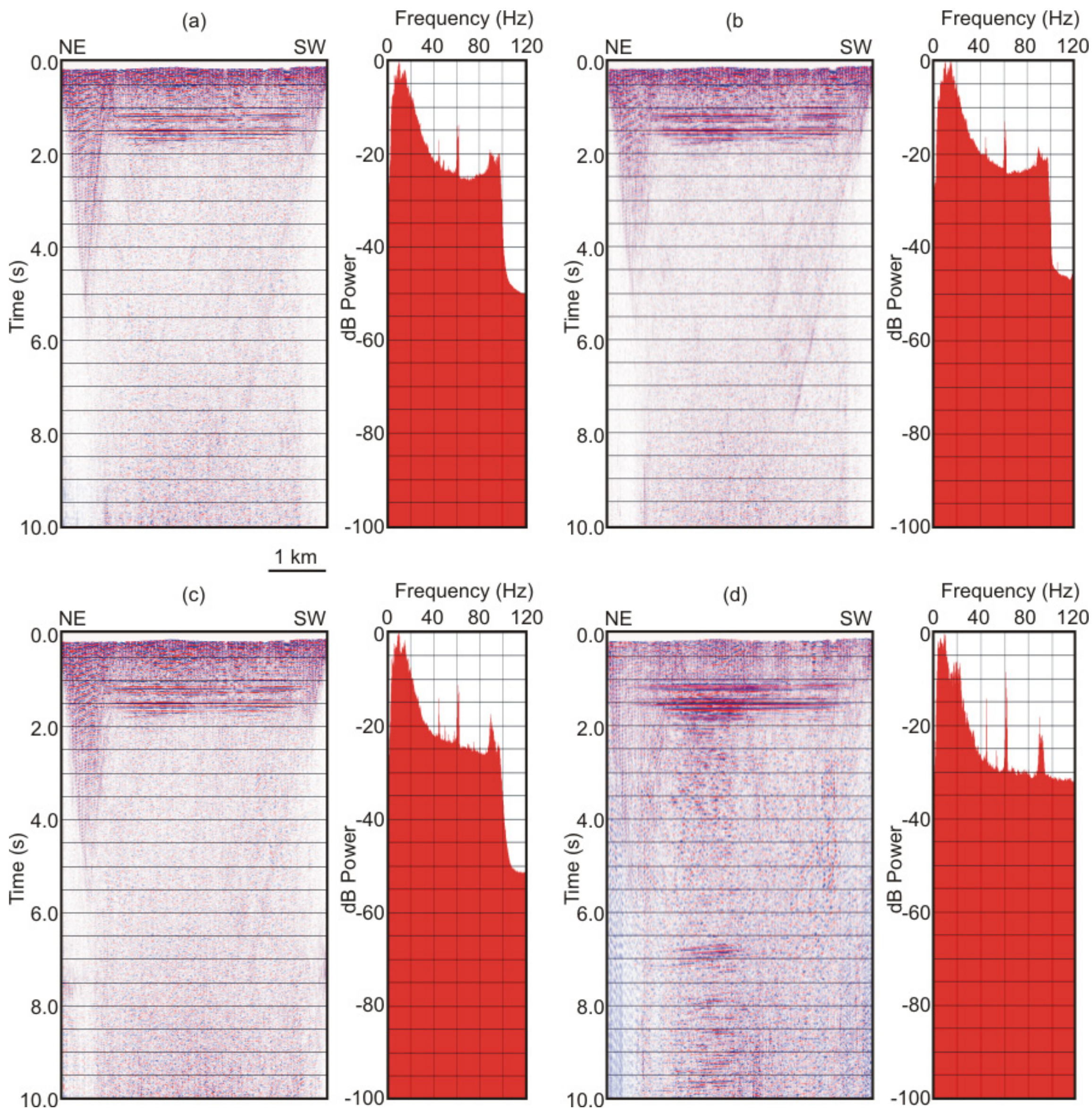

FIG. 3. Data recorded by the 4.5 Hz geophones from (a) 364 low-dwell sweep, (b) 364 linear sweep, (c) Failing low-dwell sweep and d) dynamite sources.

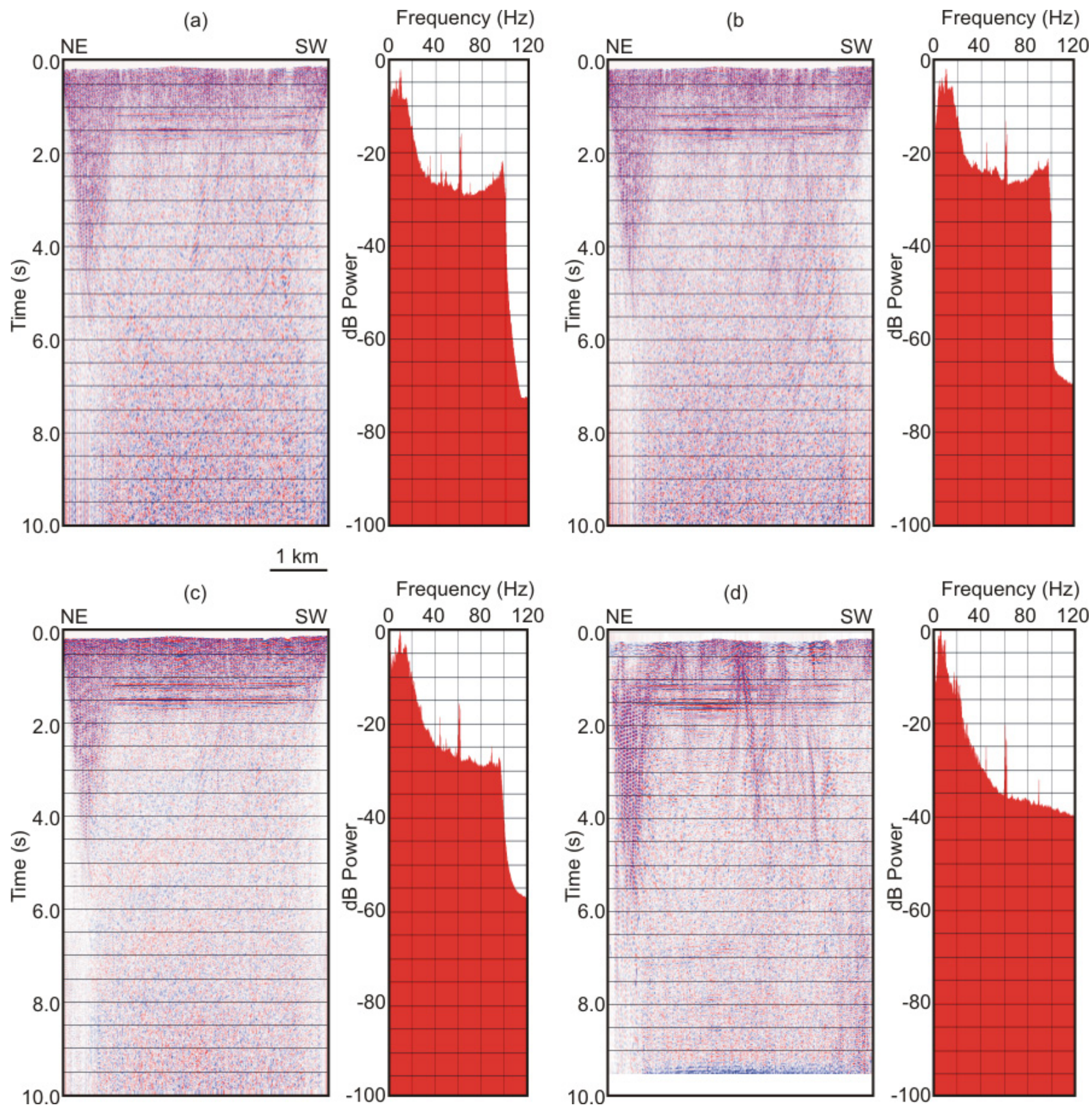

FIG. 4. Data recorded by the Vectorseis accelerometers from (a) 364 low-dwell sweep, (b) 364 linear sweep, (c) Failing low-dwell sweep and (d) dynamite sources. Noise below 9.5 s has been muted from the dynamite section.

We investigated the low frequency properties of the unfiltered stacked data by applying a bandpass filter of 0-1-10-10 Hz to each stack (Figures 5-7). A low cut of 1 Hz was applied to remove noise below that frequency. The spectra for each corresponding source show varied responses on the different recording instruments, particularly on the Vectorseis. As would be expected, the 4.5 Hz geophones have more power between 4 and 10 Hz than do the 10 Hz data and their spectra are flatter. In every case there is an increase in power from 1 Hz towards 10 Hz, but it is much more subtle on the Vectorseis data than on the geophone data. On the 10 Hz and 4.5 Hz geophones this increase is steep up to 4 Hz. The Vectorseis data show the least decrease in power between 10 Hz and 0 Hz, having an almost flat spectrum between these frequencies.

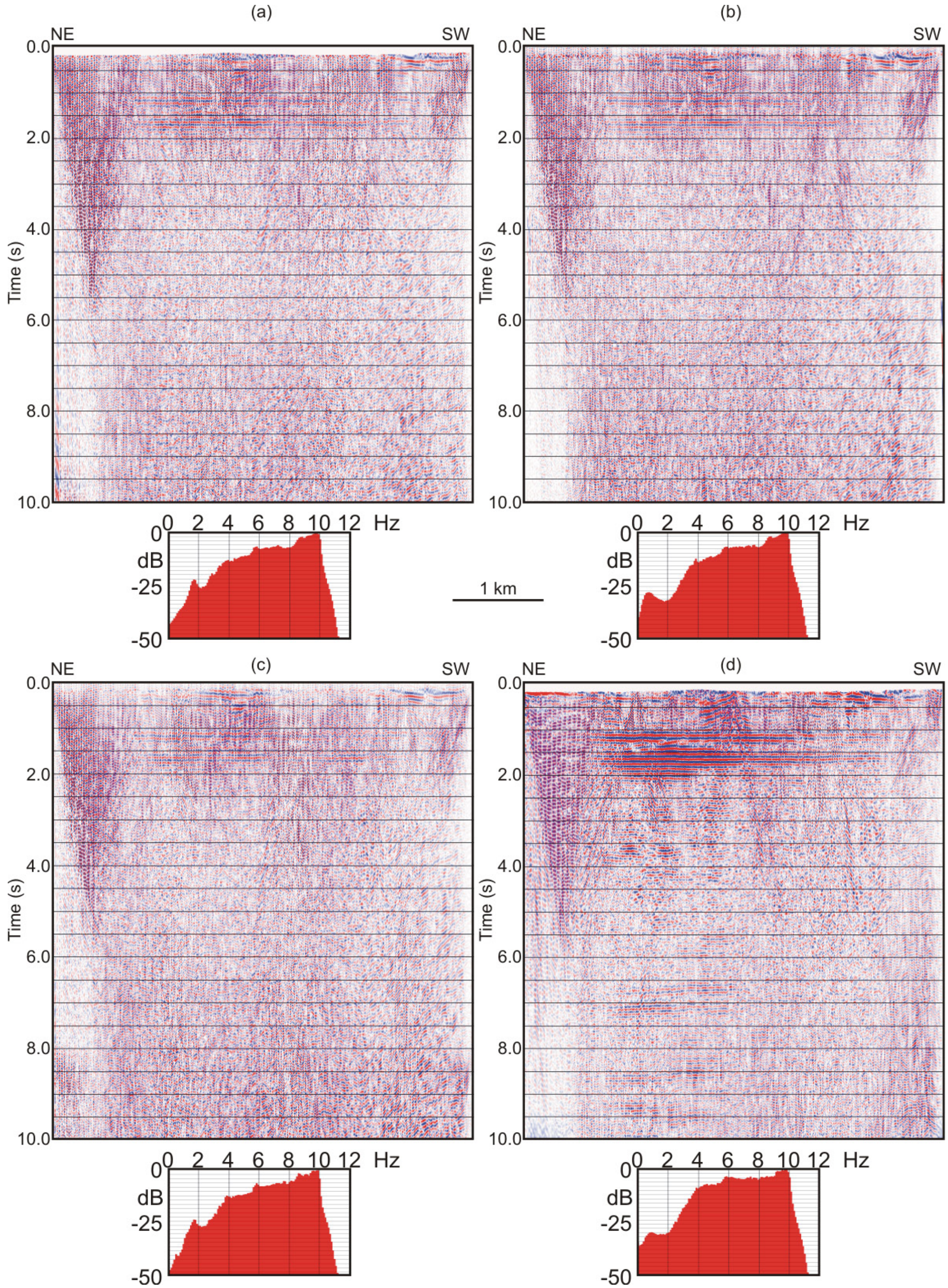

FIG.5. Stacked sections with a bandpass filter of 0-1-10-10 Hz and their spectra for data recorded by the SM7 10 Hz geophones from (a) 364 low-dwell sweep, (b) 364 linear sweep, (c) Failing low-dwell sweep and (d) dynamite sources.

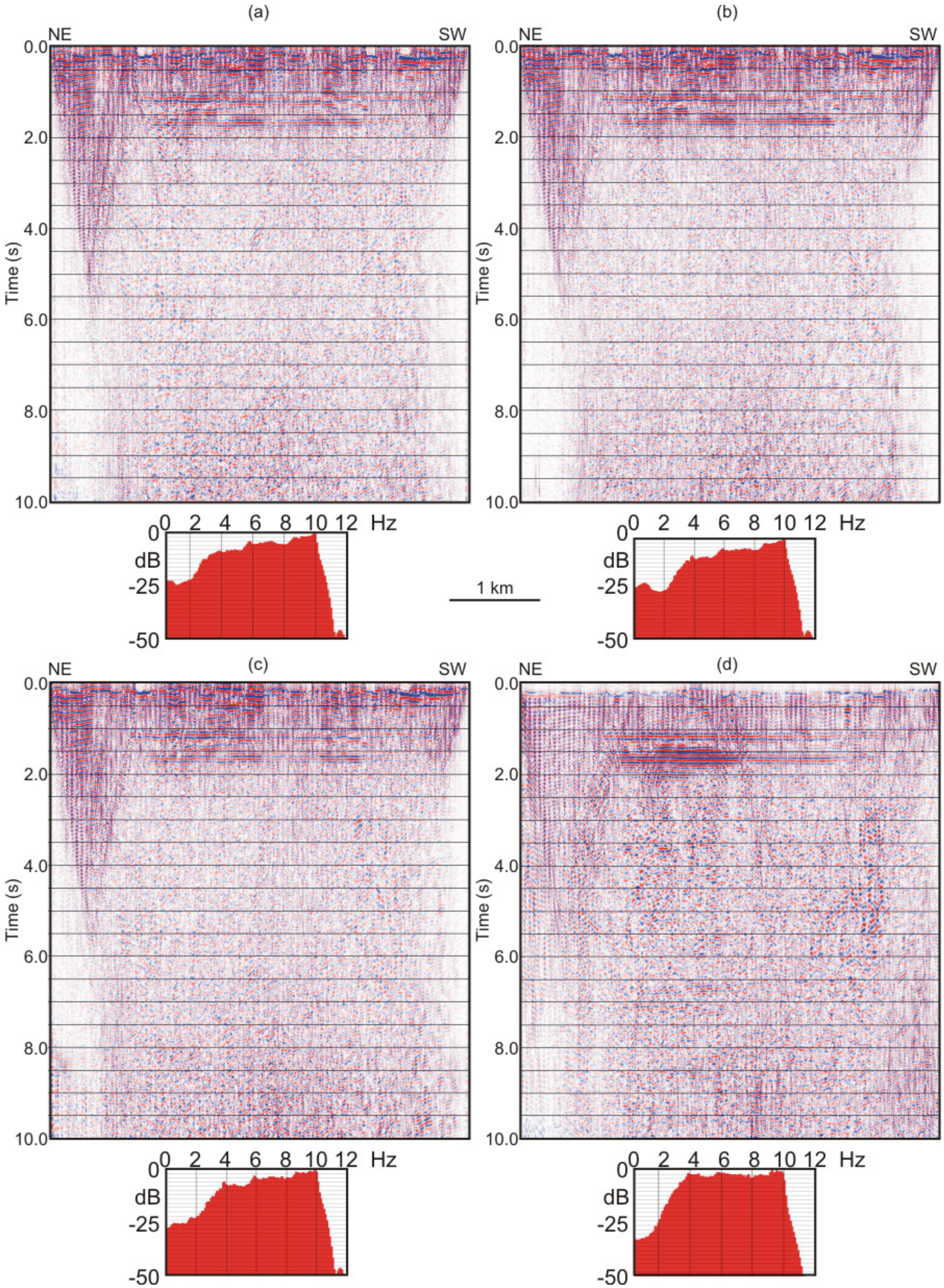

FIG. 6. Stacked sections with a bandpass filter of 0-1-10-10 Hz and their spectra for data recorded by the 4.5 Hz geophones from (a) 364 low-dwell sweep, (b) 364 linear sweep, (c) Failing low-dwell sweep and (d) dynamite sources.

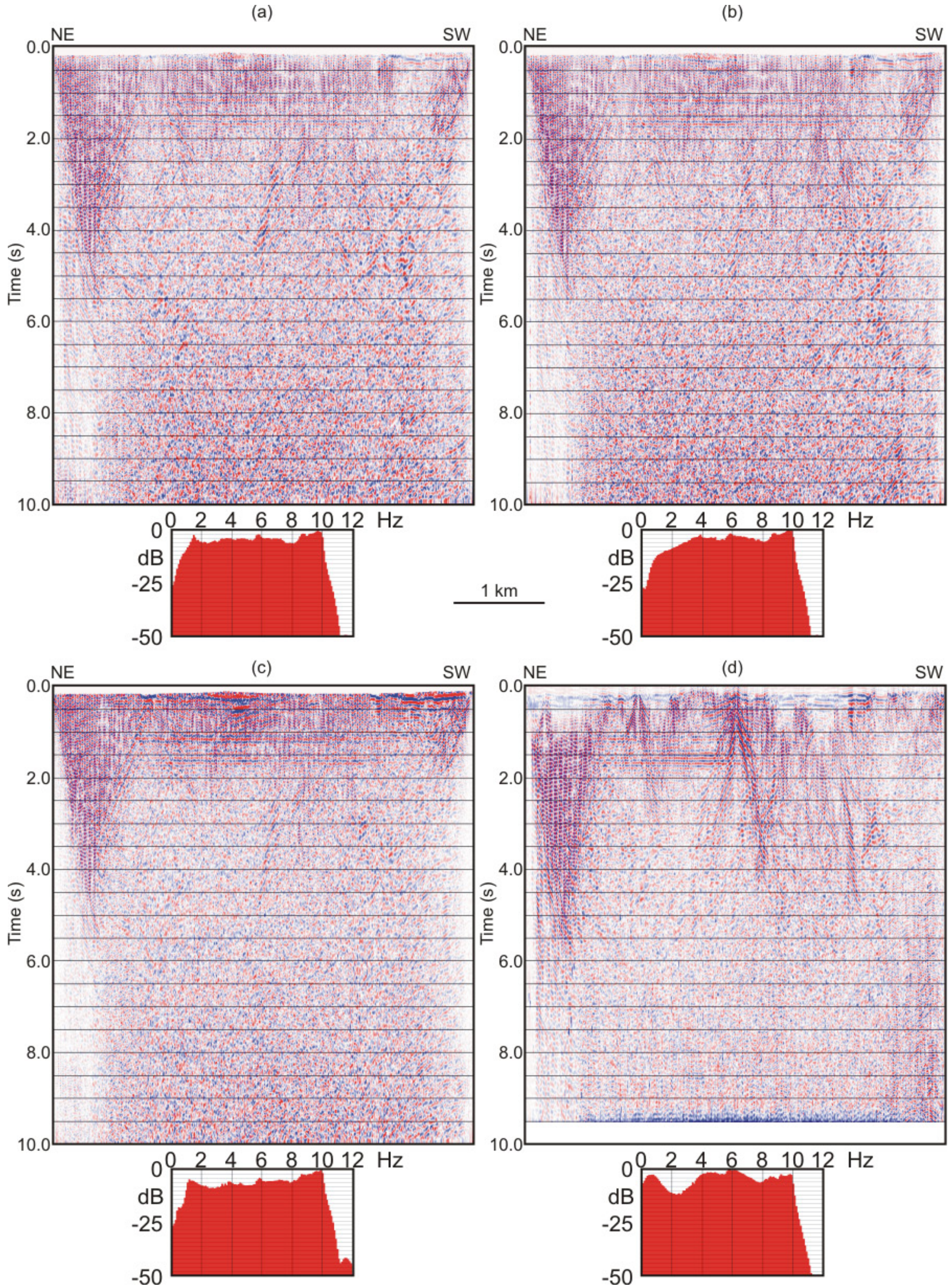

FIG. 7. Stacked sections with a bandpass filter of 0-1-10-10 Hz and their spectra for data recorded by the Vectorseis accelerometers from (a) 364 low-dwell sweep, (b) 364 linear sweep, (c) Failing low-dwell sweep and (d) dynamite sources. Noise below 9.5 s has been muted from the dynamite section.

PHASE COHERENCE ANALYSIS

We conducted a phase coherence analysis on the 12 unfiltered stacked sections. Figures 8, 9 and 10 show the results for the 10 Hz receivers, 4.5 Hz receivers and Vectorseis receivers, respectively. The spectra were all computed for the time window 0.5-2.5 s. These results show a dominant signal band that extends from about 10 Hz to 40 Hz for all sources and receivers, and possibly up to 60 Hz for the dynamite data. There is evidence of weak but definite phase coherence below 10 Hz that is, perhaps, most apparent on the Vectorseis and 4.5 Hz receivers. It is noteworthy that the dynamite has more phase coherence at the high end than any of the vibroseis.

Figures 11-13 show similar analysis designed to better examine the low-frequency phase coherence. We also conducted this analysis on the filtered data for comparison (Figures 14-16). The spectral analysis time zone was expanded to 0.5-4.0 s and the frequency axis zoomed in to 0-20 Hz.

On the unfiltered data there is phase coherence to at least 7.5 Hz and possibly to 5 Hz. It is striking that there is a very different character to the phase coherence for the dynamite source than any of the vibroseis in the zone from 10-15 Hz. The criss-crossing events below 5 Hz may be due to surface waves and these are subjects for further investigation, as are the low frequency events below 2 Hz, which may be the result of amplitude clipping in the field recording of traces close to the shots.

On the filtered data (Figure 12-15) there is phase coherence to 10 Hz and weak indications of coherence to 8 Hz. This removal of coherence between frequencies of 5 Hz and 8 Hz compared to the unfiltered data is attributed to the low frequency attenuation effects of the radial filter. Thus our conventional processing to remove undesired surface noise has adversely affected the phase-coherence analysis. There appears to be a slight advantage to having data recorded by 4.5 Hz geophones. However, we stress that we do not know how this might change with different processing. Further analysis should help us to decide the optimal combination of source and receiver for recording data to contain low frequencies.

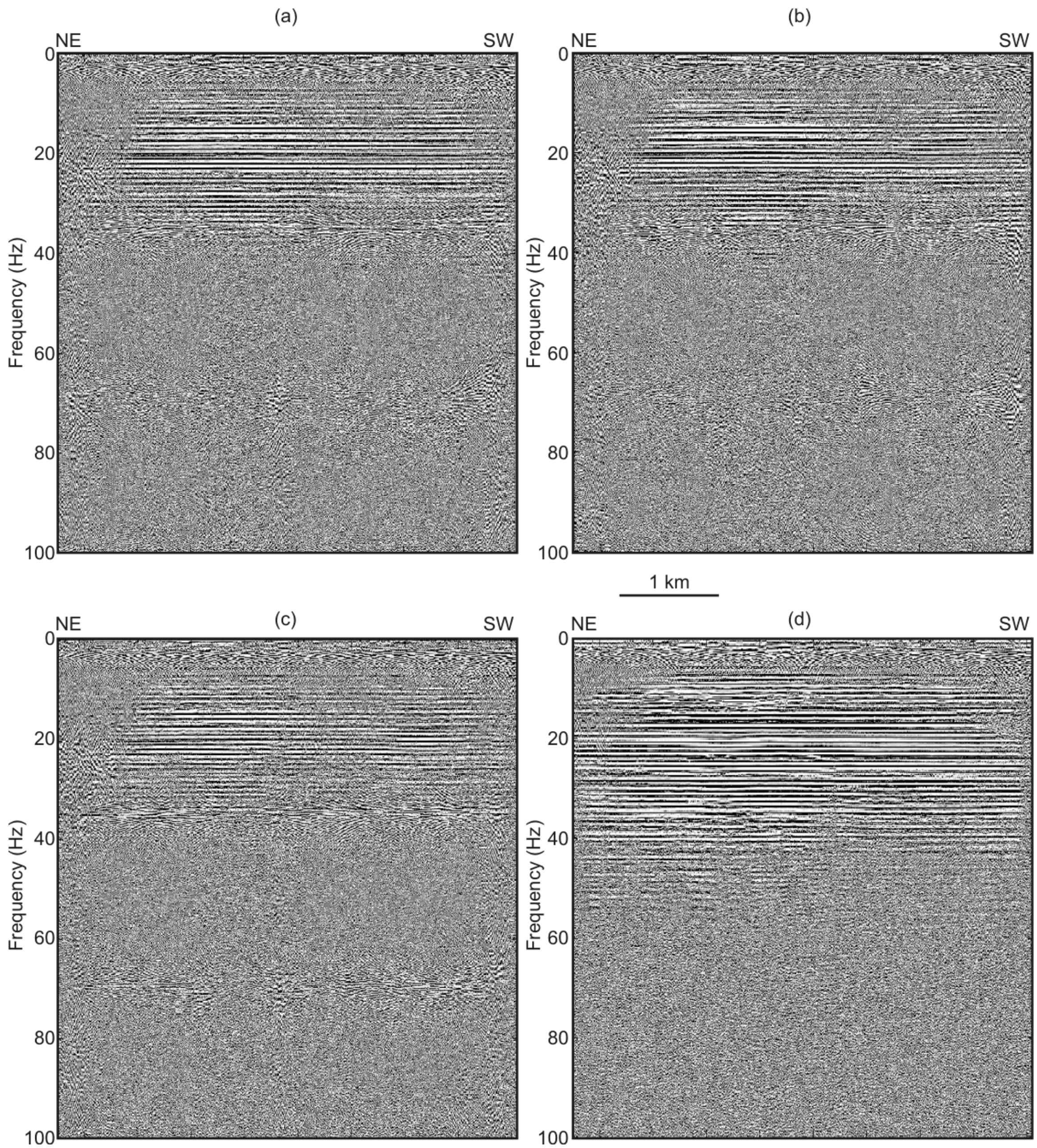

FIG. 8. Phase coherence plotted as a function of frequency and space for the 10 Hz receivers and the four different sources: (a) 364 low-dwell sweep, (b) 364 linear sweep, (c) Failing low-dwell sweep and (d) dynamite. These data have no filters applied.

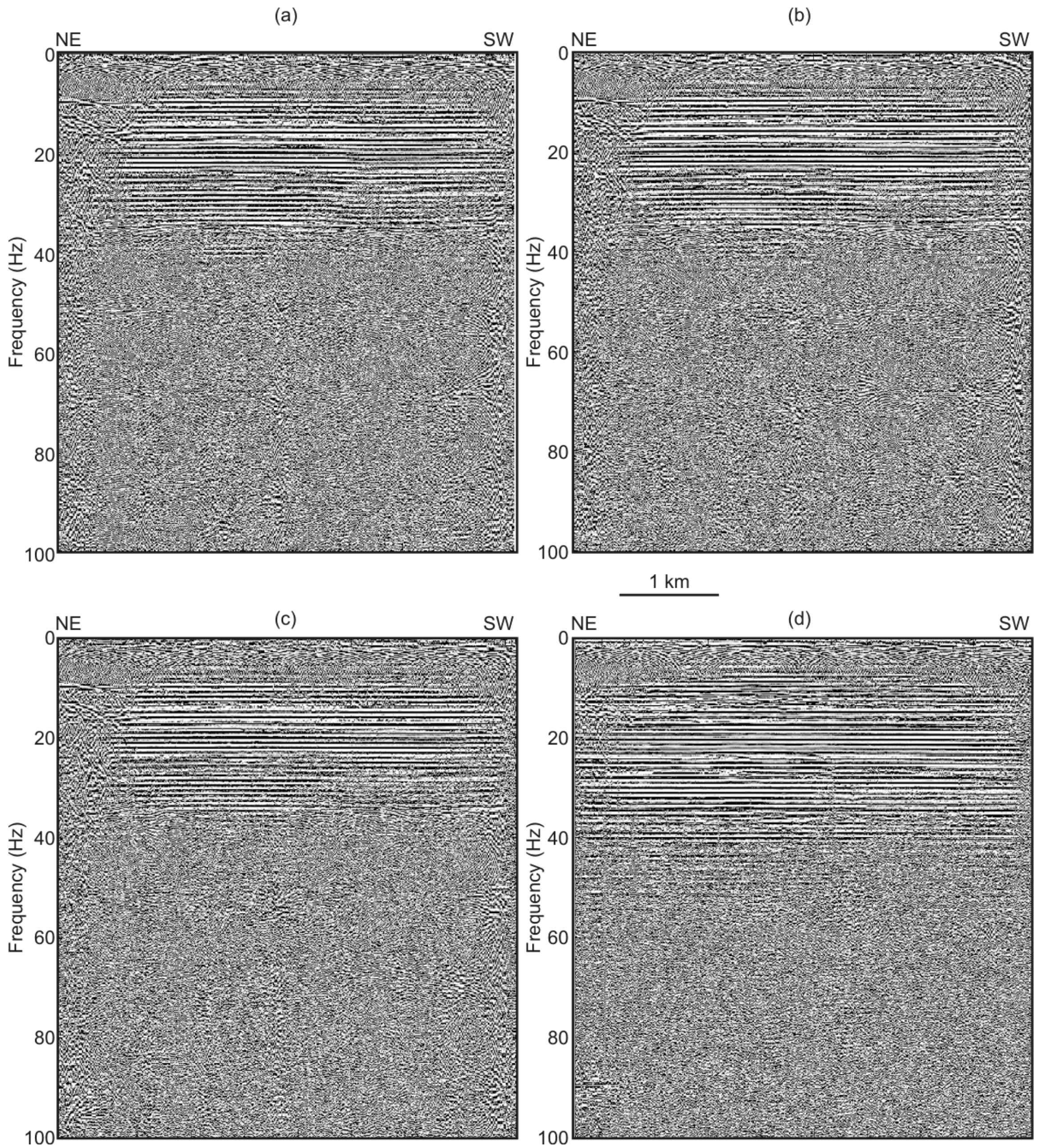

FIG. 9. Phase coherence plotted as a function of frequency and space for the 4.5 Hz receivers and the four different sources: (a) 364 low-dwell sweep, (b) 364 linear sweep, (c) Failing low-dwell sweep and (d) dynamite. These data have no filters applied.

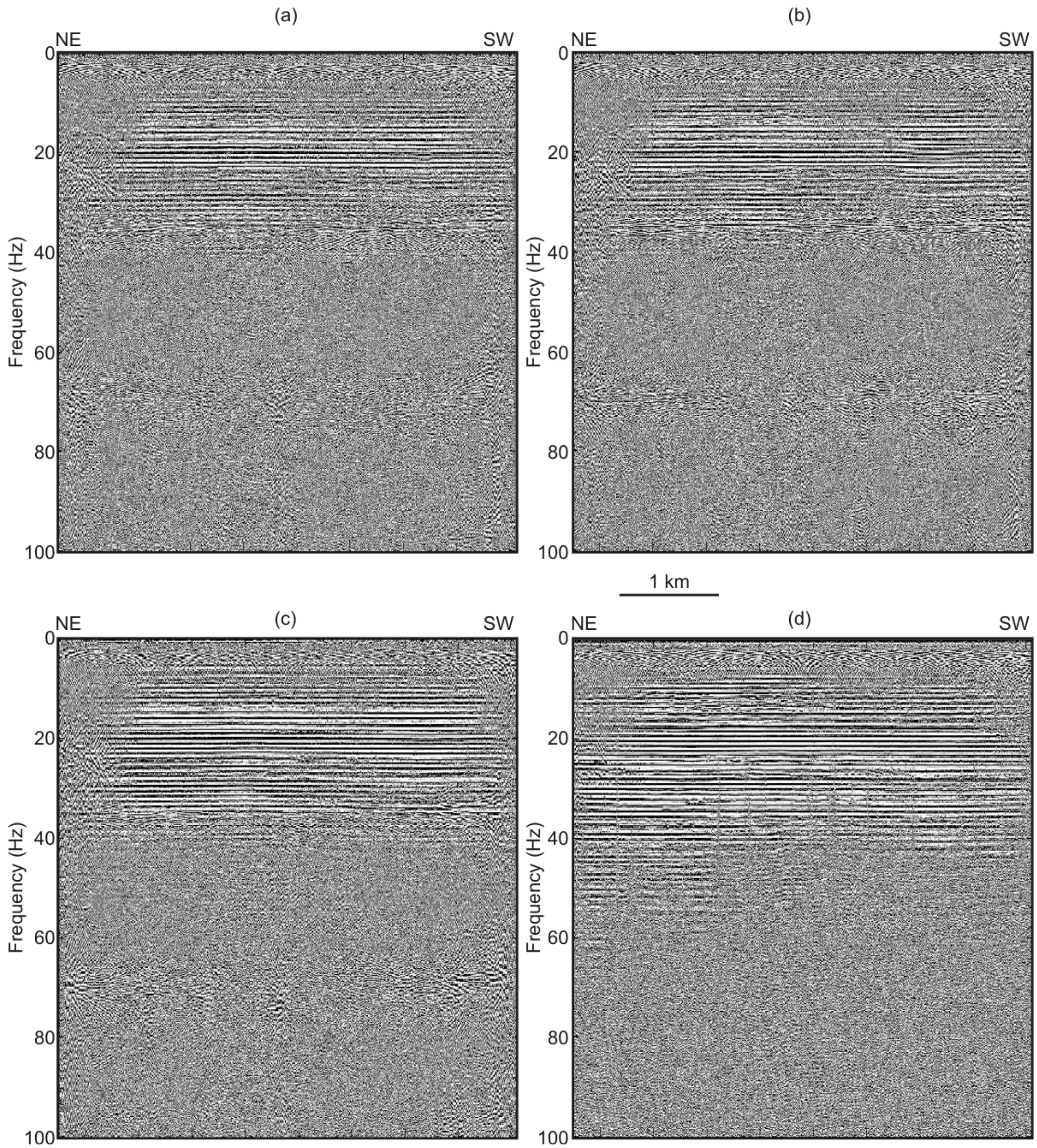

FIG. 10. Phase coherence plotted as a function of frequency and space for Vectorseis and the four different sources: (a) 364 low-dwell sweep, (b) 364 linear sweep, (c) Failing low-dwell sweep and (d) dynamite. These data have no filters applied.

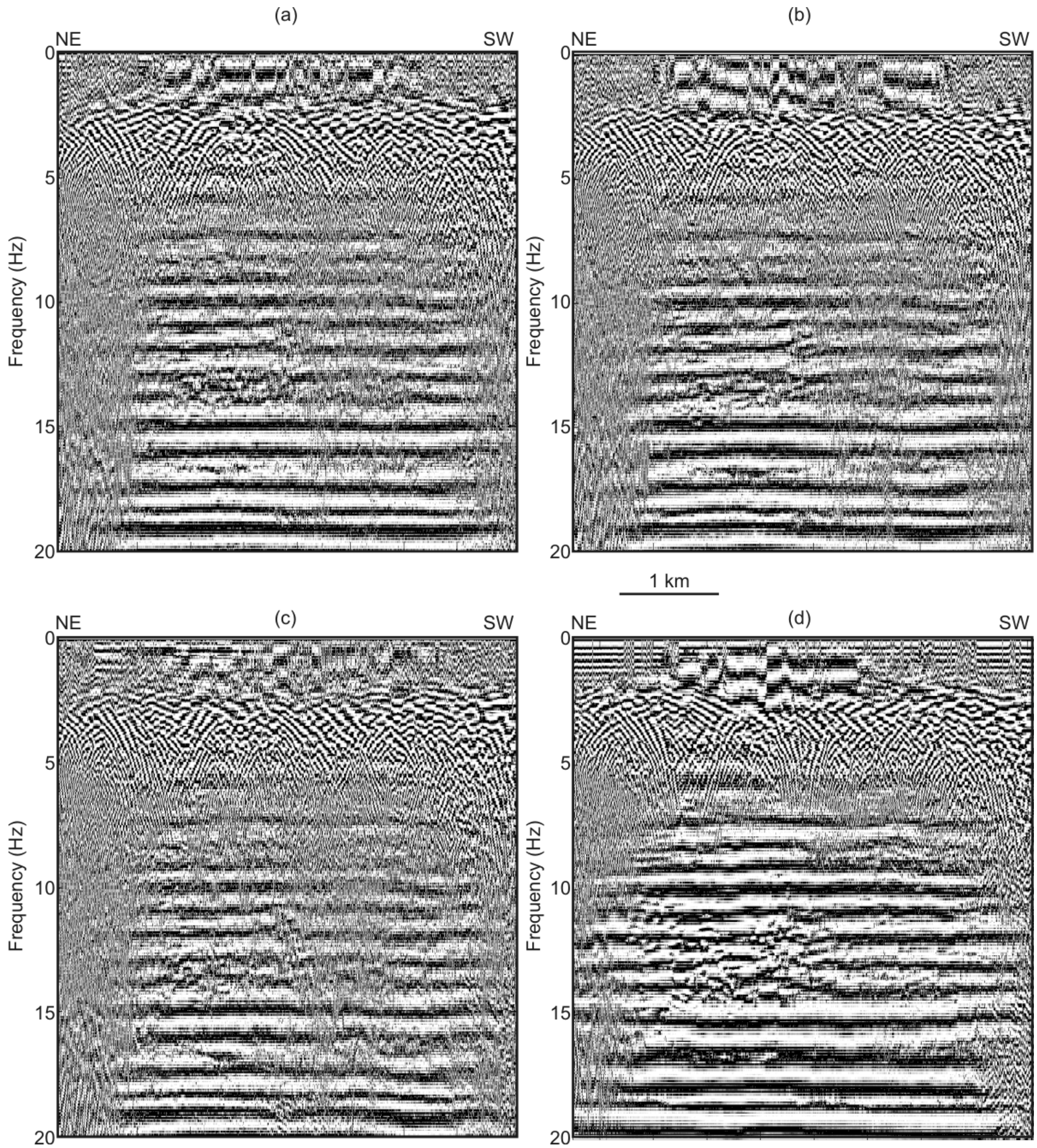

FIG. 11. Phase coherence plotted as a function of frequency and space for the 10 Hz receivers and the four different sources: (a) 364 low-dwell sweep, (b) 364 linear sweep, (c) Failing low-dwell sweep and (d) dynamite. Similar to the analysis of the 10 Hz receivers in Figure 8 but the time window was expanded from 0.5-2.5 s to 0.5-4.0 s and the frequency axis shows only 0-20 Hz. These data have no filters applied.

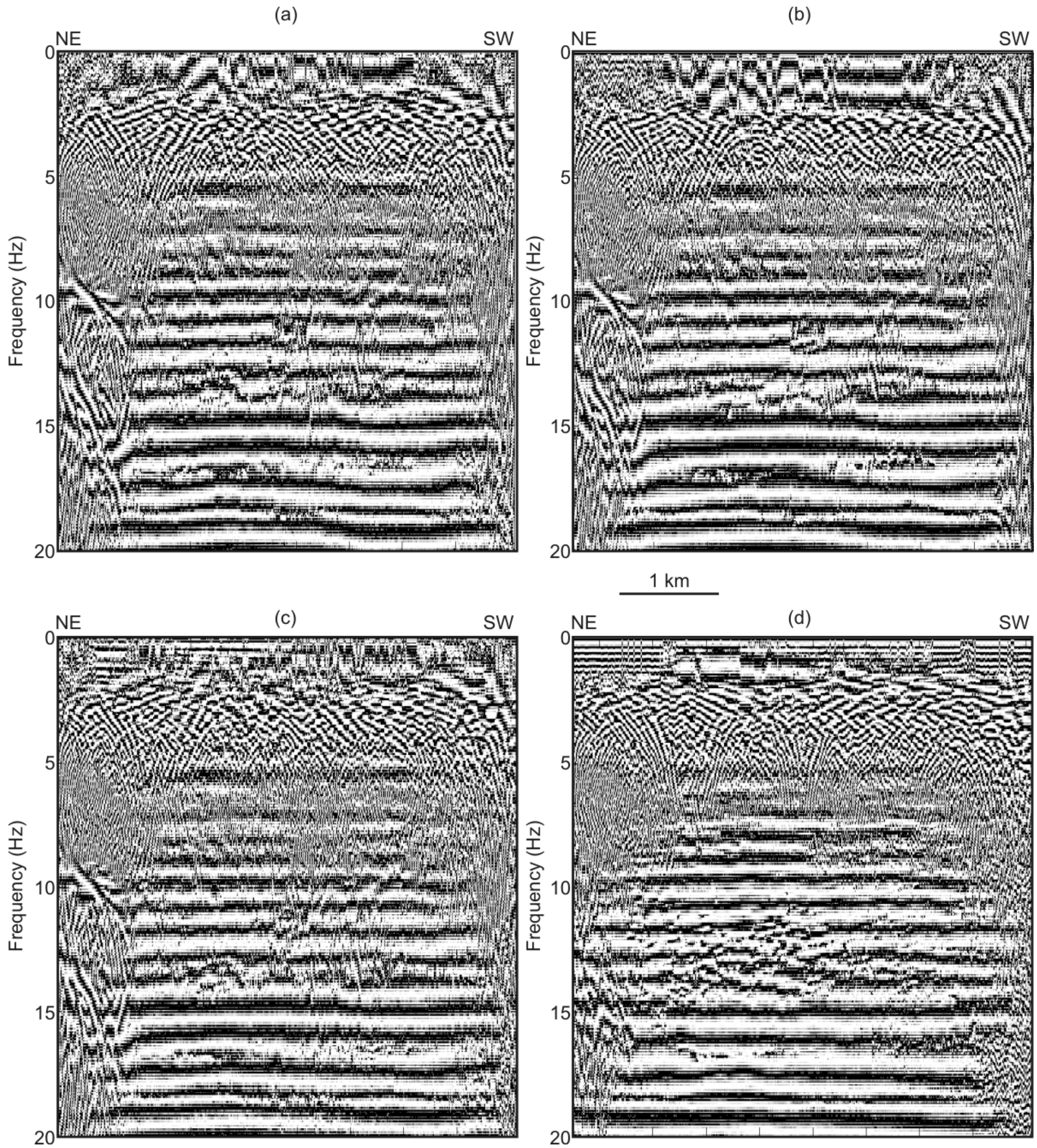

FIG. 12. Phase coherence plotted as a function of frequency and space for the 4.5 Hz receivers and the four different sources: (a) 364 low-dwell sweep, (b) 364 linear sweep, (c) Failing low-dwell sweep and (d) dynamite. Similar to the analysis of the 4.5 Hz receivers in Figure 9 but the time window was expanded from 0.5-2.5 s to 0.5-4.0 s and the frequency axis shows only 0-20 Hz. These data have no filters applied.

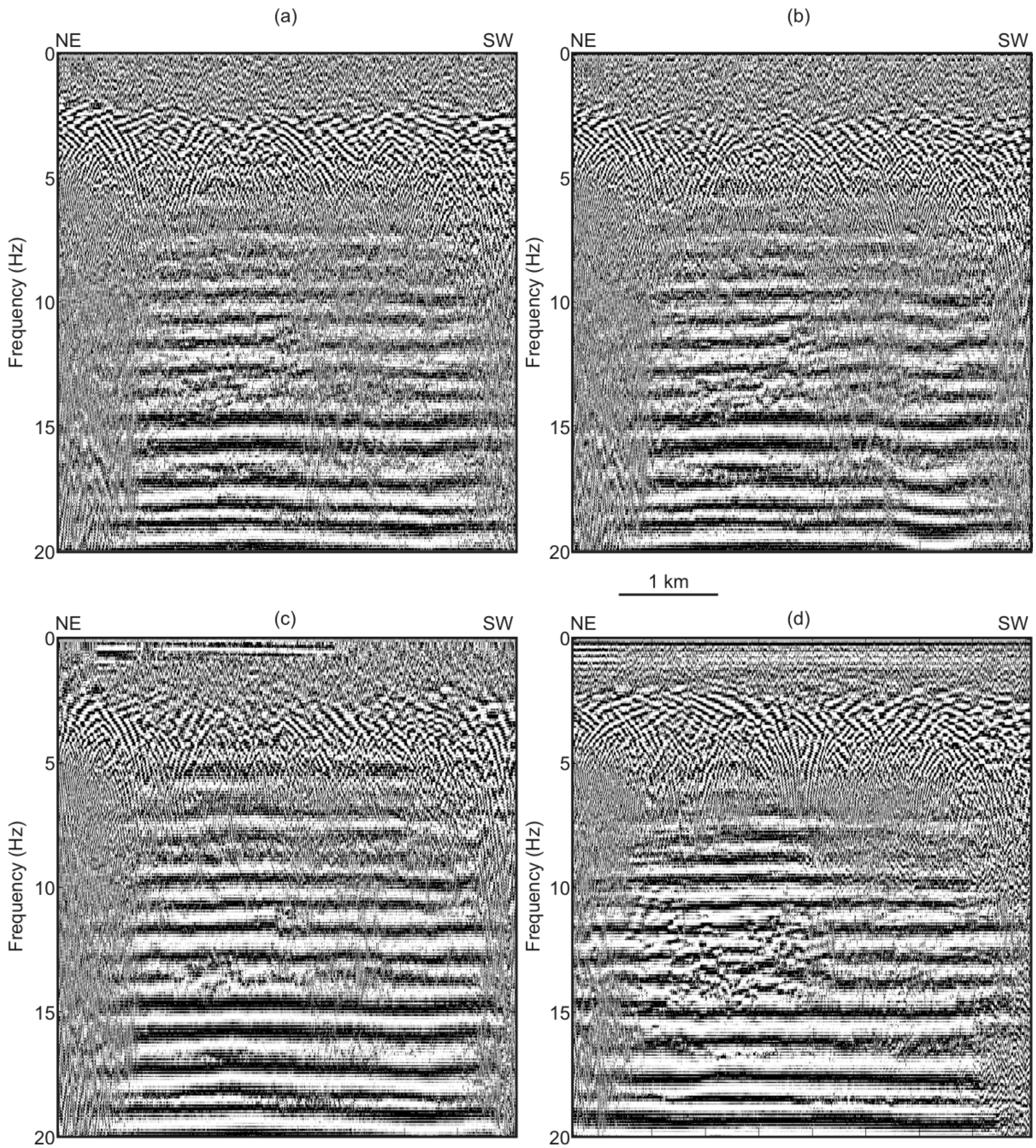

FIG. 13. Phase coherence plotted as a function of frequency and space for the Vectorseis receivers and the four different sources: (a) 364 low-dwell sweep, (b) 364 linear sweep, (c) Failing low-dwell sweep and (d) dynamite. Similar to the analysis of the Vectorseis receivers in Figure 10 but the time window was expanded from 0.5-2.5 s to 0.5-5.0 s and the frequency axis shows only 0-20 Hz. These data have no filters applied.

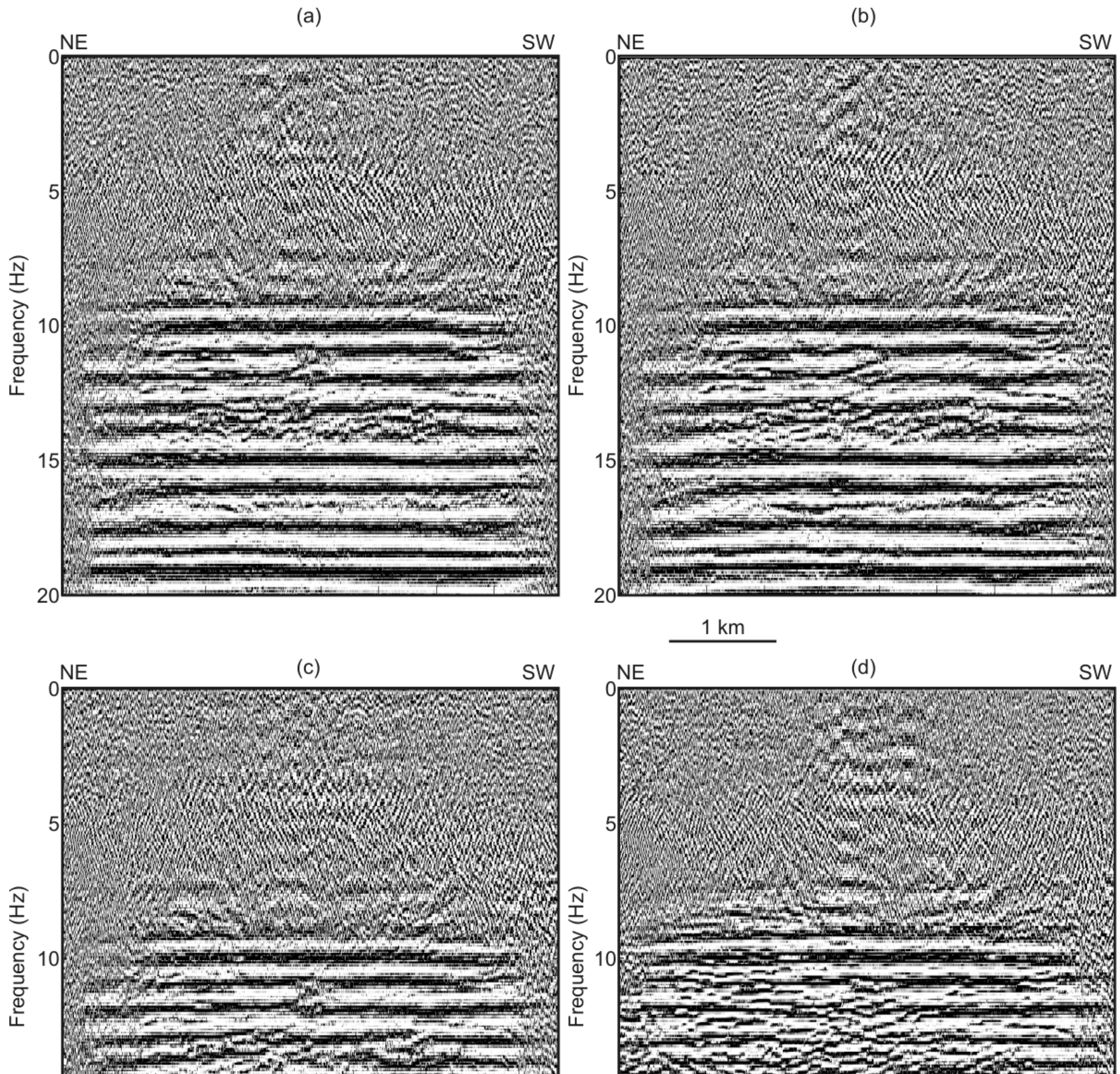

FIG. 14. Phase coherence plotted as a function of frequency and space for the 10 Hz receivers and the four different sources: (a) 364 low-dwell sweep, (b) 364 linear sweep, (c) Failing low-dwell sweep and (d) dynamite. Similar to the analysis in Figure 11 except these data have radial filtering and Gabor deconvolution applied.

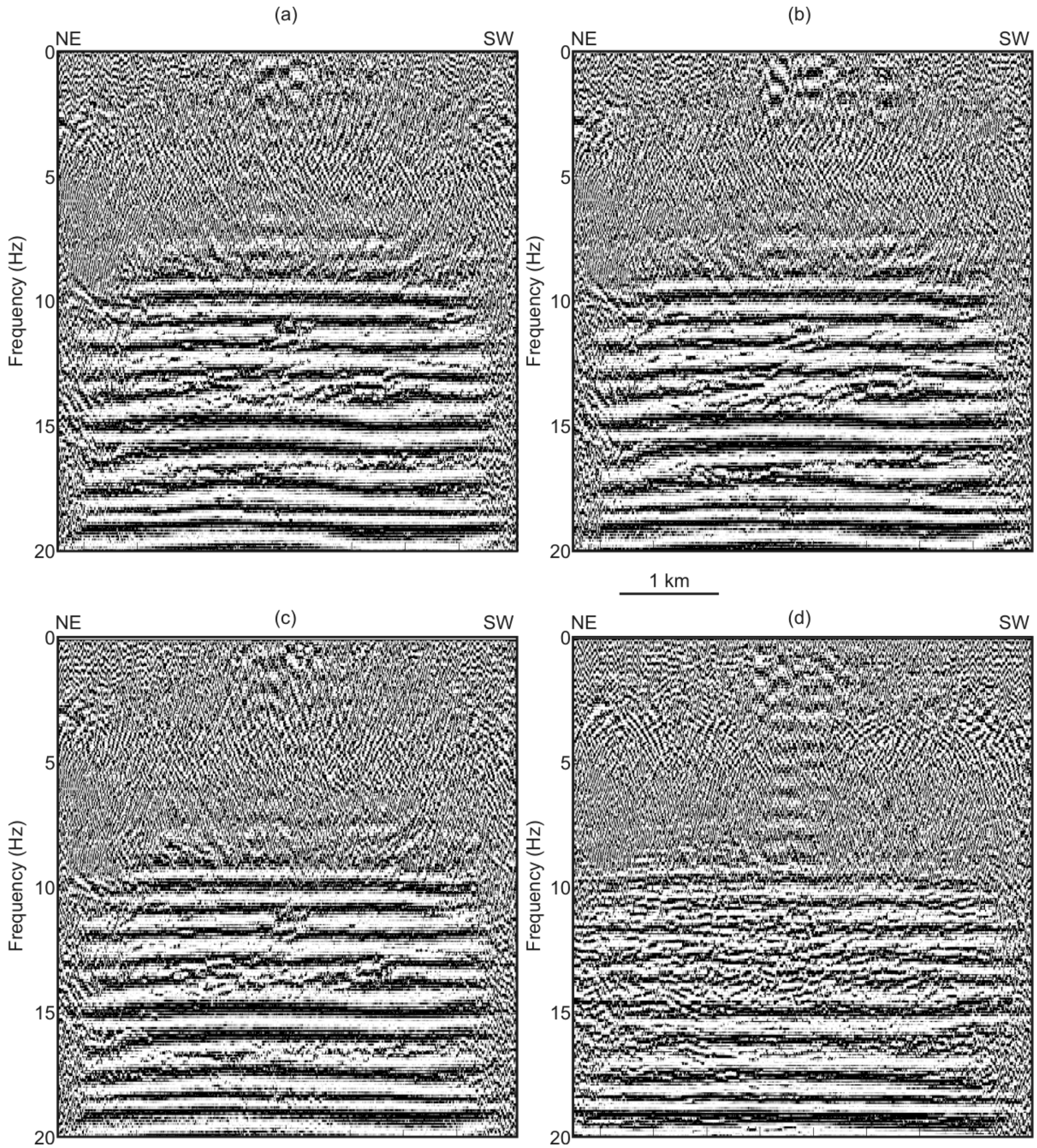

FIG. 15. Phase coherence plotted as a function of frequency and space for the 4.5 Hz receivers and the four different sources: (a) 364 low-dwell sweep, (b) 364 linear sweep, (c) Failing low-dwell sweep and (d) dynamite. Similar to the analysis in Figure 12 except these data have radial filtering and Gabor deconvolution applied.

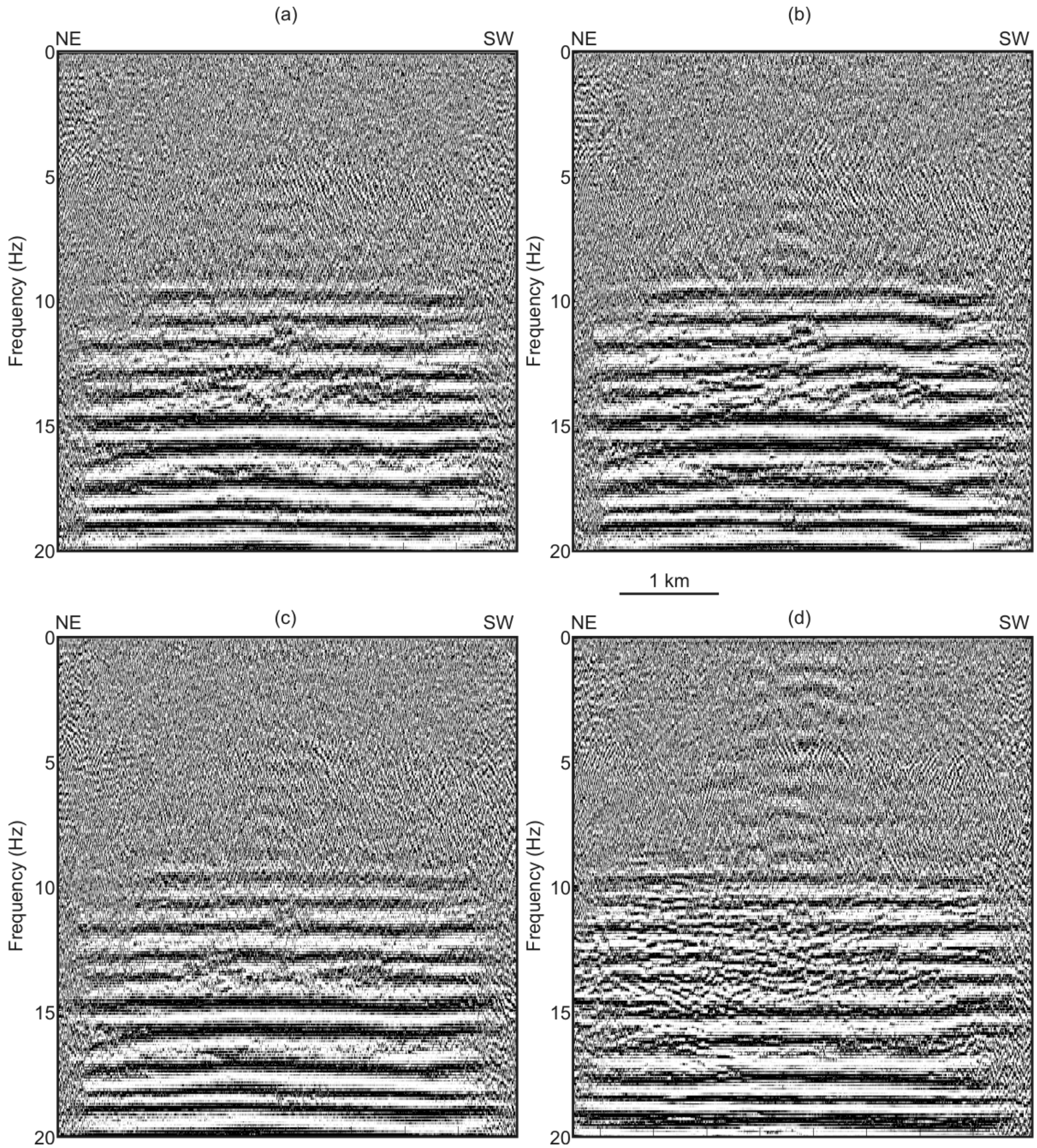

FIG. 16. Phase coherence plotted as a function of frequency and space for the Vectorseis receivers and the four different sources: (a) 364 low-dwell sweep, (b) 364 linear sweep, (c) Failing low-dwell sweep and (d) dynamite. Similar to the analysis in Figure 13 except these data have radial filtering and Gabor deconvolution applied.

POST-STACK TIME MIGRATIONS

We poststack migrated all the data with radial filter and Gabor deconvolution applied. Figures 17, 18, 19 and 20 show the post-stack migrations of the 364 low dwell sweep vibroseis, 364 linear sweep vibroseis, Failing low dwell sweep vibroseis and the dynamite data, respectively. In each figure (a) was recorded by the 3C geophones, (b) by the 4.5 Hz geophones and (c) by the Vectorseis accelerometers. In these figures we show only the first 2 s of data, covering the area of economic interest. The vibroseis data appear to have an unresolved statics issue to the SW end of the line which is better resolved in the dynamite data. The vibroseis sections all have very similar character apart from some minor differences between 1 s and 1.2 s, while the dynamite data differ slightly throughout the section. However, the processing was not designed to investigate this shallow part of the section but rather to analyze the frequency properties of the different data sets.

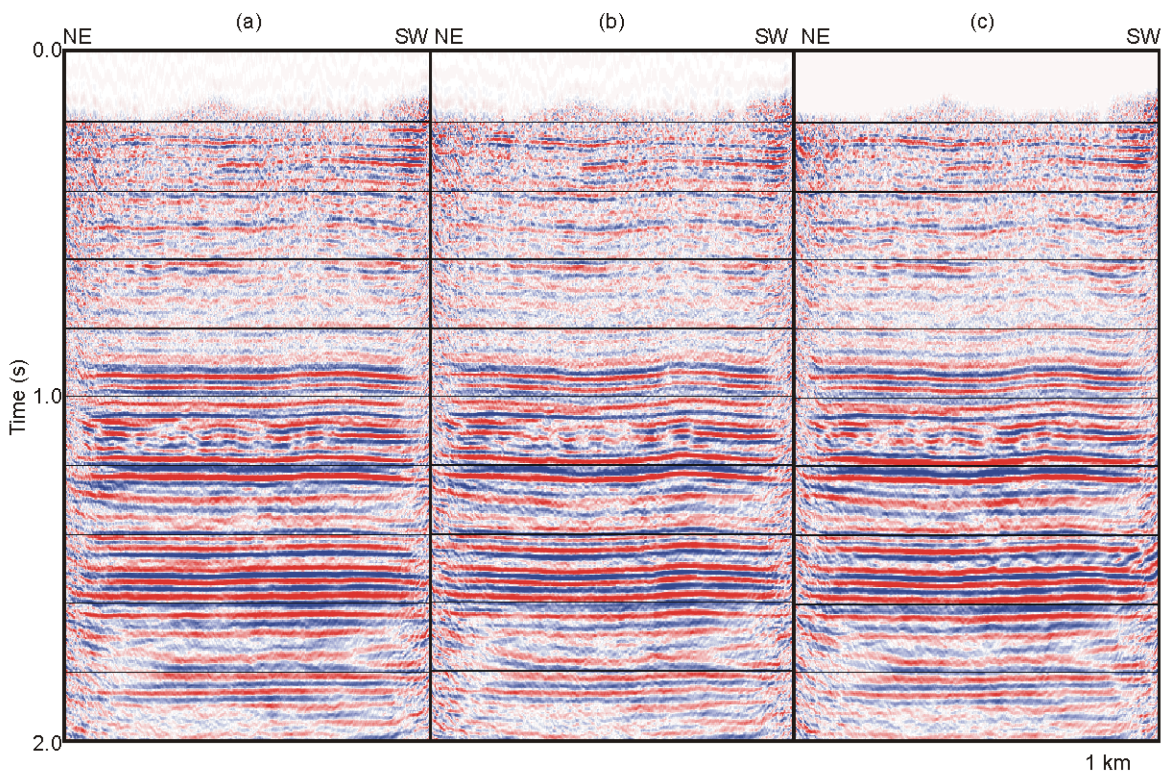

FIG. 17. Poststack migrated sections of the 364 low-dwell sweep vibroseis data recorded by the (a) 10 Hz geophones, (b) 4.5 Hz geophones and (c) Vectorseis accelerometers.

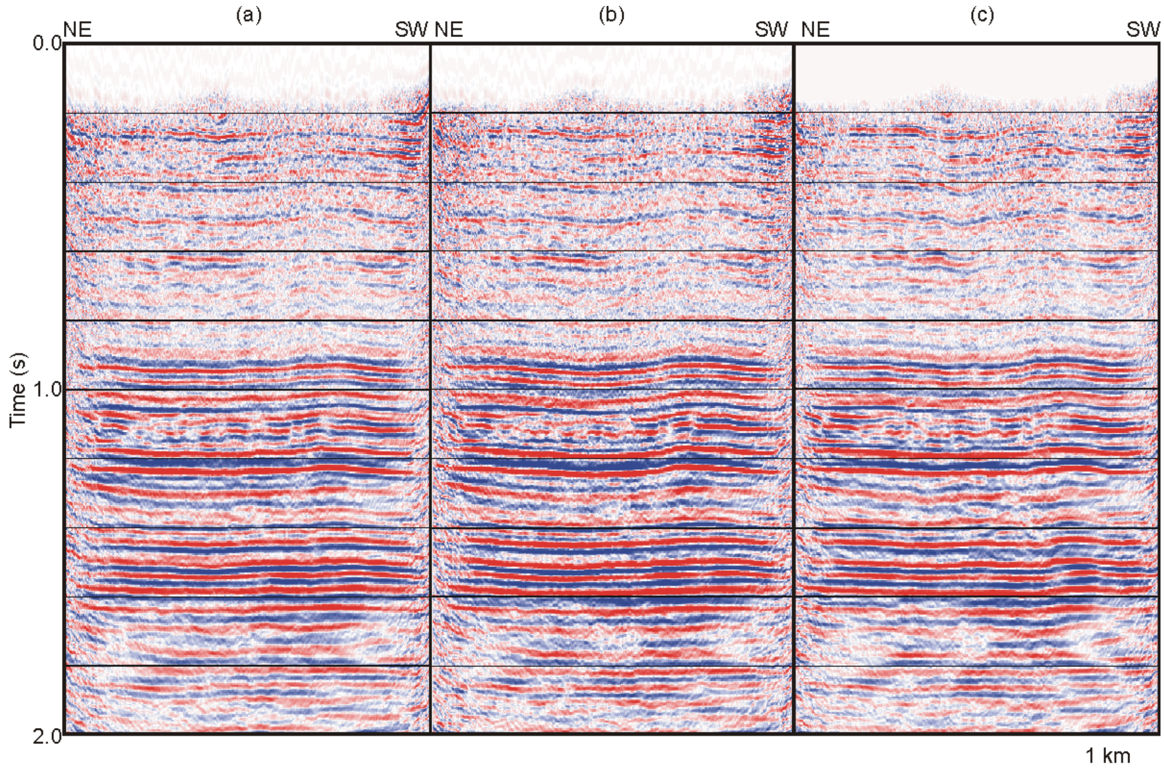

FIG. 18. Poststack migrated sections of the 364 linear sweep vibroseis data recorded by the (a) 10 Hz geophones, (b) 4.5 Hz geophones and (c) Vectorseis accelerometers.

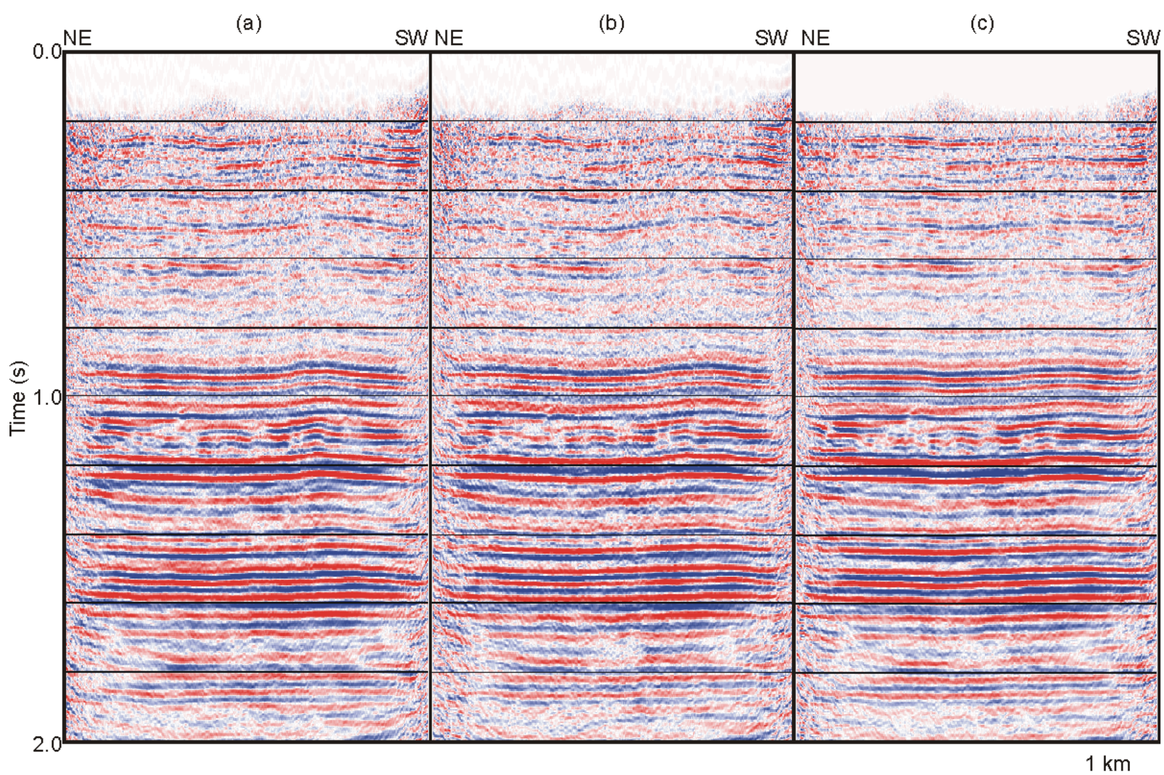

FIG. 19. Poststack migrated sections of the Failing low-dwell sweep vibroseis data recorded by the (a) 10 Hz geophones, (b) 4.5 Hz geophones and (c) Vectorseis accelerometers.

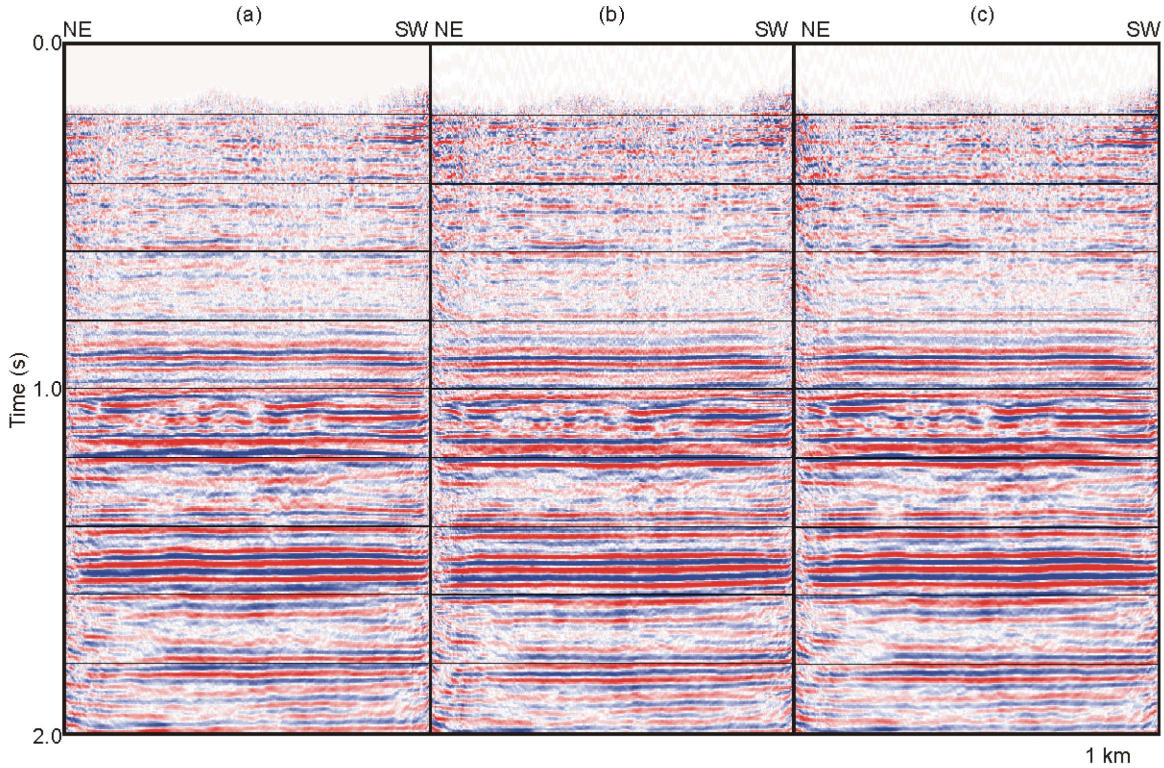

FIG. 20. Poststack migrated sections of the dynamite data recorded by the (a) 10 Hz geophones, (b) 4.5 Hz geophones and (c) Vectorseis accelerometers.

SUMMARY

We processed, stacked and post-stack migrated twelve data sets having combinations of four different sources and three different receiver types. The post-stack time migrated vibroseis data show only minor differences in the character of reflections in shallow section above 2 s, but the dynamite data have slightly different character.

We investigated the low frequency properties of the unfiltered stacked data by applying a bandpass filter of 0-1-10-10 Hz to each stack. The spectra for each corresponding source show varied responses on the different recording instruments, particularly on the Vectorseis. The 4.5 Hz geophones have more power between 4 and 10 Hz than do the 10 Hz data and their spectra are flatter. In every case there is an increase in power towards 10 Hz. On the 10 Hz and 4.5 Hz geophones this increase is steep up to 4 Hz while the Vectorseis data show the least drop in power between 10 Hz and 0 Hz, having an almost flat spectrum between these frequencies.

Phase coherence analysis on the 12 unfiltered stacked sections show a dominant signal band that extends from about 10 Hz to 40 Hz for all sources and receivers, and possibly up to 60 Hz for the dynamite data. The dynamite has more phase coherence at the high end than any of the vibroseis. On the unfiltered data there is phase coherence to at least 7.5 Hz and possibly to 5 Hz. On the filtered data there is phase coherence to 10 Hz and weak indications of coherence to 8 Hz. This removal of coherence between frequencies of 5 Hz and 8 Hz compared to the unfiltered data is attributed to the low frequency attenuation effects of the radial filter. Thus our conventional; processing to remove undesired surface noise appears to have adversely affected the phase-coherence analysis.

Future work will include investigation of how different filters affect the frequency analysis, in particular those filters that attenuate undesired surface wave noise.

ACKNOWLEDGEMENTS

We are very grateful to the companies that made this experiment possible: Husky Energy, Geokinetics, INOVA, ION-Sensor. We also thank the CREWES sponsors and Carbon Management Canada for funding and Landmark Graphics for ProMAX processing software.

REFERENCES

Henley, D. C., 1999, Coherent noise attenuation in the radial trace domain: Introduction and demonstration: CREWES Research Report, Vol. **11**, Ch. 36.

Margrave, G. F. and M. P. Lamoureux, 2002, Gabor deconvolution: 2002 CSEG Annual Convention, Calgary, AB.

Margrave G. F., L. Dong, P. Gibson, J. P Grossman, D. Henley and M. P. Lamoureux, 2003, Gabor deconvolution: Extending Wiener's Method to nonstationarity: CREWES Research Report, Vol. **15**.

Margrave, G. F., M. B. Bertram, D. C. Lawton, K. A. H. Innanen, K. W. Hall, L. Mewhort and M. Hall, 2011, The Hussar Low-Frequency Experiment: CREWES Research Report, Vol. **23**.